International Immunopharmacology 120 (2023) 110351

Contents lists available at ScienceDirect

International Immunopharmacology

journal homepage: www.elsevier.com/locate/intimp

Cyclophilins modify their profile depending on the organ or tissue in a murine inflammatory model

Sandra Gegunde [a,b], Amparo Alfonso [a,b,*], J. Manuel Cifuentes [c], Rebeca Alvariño [a,b], Nadia Pérez-Fuentes [a,b], Mercedes R. Vieytes [d], Luis M. Botana [a,b,*]

[a] Departamento de Farmacología, Facultad de Veterinaria, Universidad de Santiago de Compostela, 27002 Lugo, Spain
[b] Grupo de investigación Biodiscovery (IDIS), Lugo, Spain
[c] Departamento de Anatomía, Producción Animal y Ciencias Clínicas Veterinarias, Facultad de Veterinaria, Universidad de Santiago de Compostela, 27002 Lugo, Spain
[d] Departamento de Fisiología, Facultad de Veterinaria, Universidad de Santiago de Compostela, 27002 Lugo, Spain

ARTICLE INFO

Keywords:
Inflammation
Cyclophilins
CD147 receptor
Aorta
Kidney
Liver
Cyclophilin A inhibitor

ABSTRACT

Inflammation is the leading subjacent cause of many chronic diseases. Despite several studies in the last decades, the molecular mechanism involving its pathophysiology is not fully known. Recently, the implication of cyclophilins in inflammatory-based diseases has been demonstrated. However, the main role of cyclophilins in these processes remains elusive. Hence, a mouse model of systemic inflammation was used to better understand the relationship between cyclophilins and their tissue distribution. To induce inflammation, mice were fed with high-fat diet for 10 weeks. In these conditions, serum levels of interleukins 2 and 6, tumour necrosis factor-α, interferon-ϒ, and the monocyte chemoattractant protein 1 were elevated, evidencing a systemic inflammatory state. Then, in this inflammatory model, cyclophilins and CD147 profiles in the aorta, liver, and kidney were studied. The results demonstrate that, upon inflammatory conditions, cyclophilins A and C expression levels were increased in the aorta. Cyclophilins A and D were augmented in the liver, meanwhile, cyclophilins B and C were diminished. In the kidney, cyclophilins B and C levels were elevated. Furthermore, CD147 receptor was also increased in the aorta, liver, and kidney. In addition, when cyclophilin A was modulated, serum levels of inflammatory mediators were decreased, indicating a reduction in systemic inflammation. Besides, the expression levels of cyclophilin A and CD147 were also reduced in the aorta and liver, when cyclophilin A was modulated. Therefore, these results suggest that each cyclophilin has a different profile depending on the tissue, under inflammatory conditions.

1. Introduction

Currently, inflammation is a common component of many diseases. In this sense, in recent decades it has been raised that inflammation is the leading cause of diverse pathologies or chronic disorders, including cancer, diabetes, cardiovascular diseases, neurodegenerative disorders, and arthritis, among others. These conditions share a low-grade systemic inflammatory basis, and their origin remains unclear [1,2]. Many factors can contribute to the inflammatory process, including genetic predisposition, oxidative stress, mitochondrial dysfunction, and diet [3,4]. Moreover, recent data have evidenced an important role of cyclophilins (Cyps) in the pathophysiology of inflammation [5,6]. Cyps belong to the peptidyl-prolyl cis–trans isomerase (PPIase) family and are proteins ubiquitously expressed in all cells. They are involved in important cellular processes, including protein folding, signalling, transcriptional regulation, and cell cycle regulation [5,7]. Among these proteins, CypA, B, C, and D are implicated in the development of inflammation and play a key role in numerous inflammatory-related diseases [5].

CypA is the most abundant member of the immunophilin family, found in the cytosol and the cell nucleus. CypA participates in the inflammatory process through the activation of gene transcription and cytokine formation [8]. CypB is highly expressed in all tissues, although at a lower level than CypA [6]. Moreover, CypB is mainly located in the endoplasmic reticulum (ER) and Golgi apparatus, where it is essential in redox and calcium homeostasis [9]. CypC is less abundant than CypA and CypB and is distributed differently in tissues since higher expression of CypC has been observed in the kidney [10]. This protein, like CypB, regulates ER redox homeostasis and protein assembling and excretion

* Corresponding authors at: Departamento de Farmacología, Facultad de Veterinaria, Universidad de Santiago de Compostela, 27002 Lugo, Spain.
E-mail addresses: amparo.alfonso@usc.es (A. Alfonso), luis.botana@usc.es (L.M. Botana).

https://doi.org/10.1016/j.intimp.2023.110351
Received 15 February 2023; Received in revised form 10 May 2023; Accepted 13 May 2023
Available online 24 May 2023
1567-5769/© 2023 The Author(s). Published by Elsevier B.V. This is an open access article under the CC BY-NC-ND license (http://creativecommons.org/licenses/by-nc-nd/4.0/).

[9]. Furthermore, CypD is a component of the mitochondrial pore and is related to mitochondrial dysfunction and oxidative damage in neurodegenerative, autoimmune, and inflammatory diseases [11]. Upon oxidative stress or inflammatory stimuli, Cyps could be released to the extracellular media. In this sense, high extracellular Cyps levels were related to several inflammatory pathologies. Moreover, increased CypA levels were found in patients with sepsis or diabetes [12]. Meanwhile, high serum levels of CypB were associated with metabolic syndrome or asthma [13]. In addition, elevated CypA, B, and C serum levels have been detected in patients with coronary artery disease [5,14,15]. The extracellular functions of Cyps are mediated by their binding to the plasma membrane receptor CD147. Consequently, Cyp-CD147 interaction participates in the inflammatory response development [16,17]. In this sense, extracellular CypA and B act as chemoattractants for leukocytes and as a modulator of proinflammatory cytokine production, intensifying the inflammation via CD147 receptor [18,19]. Although the pro-inflammatory properties of Cyps are widely documented, the exact role of these proteins in inflammatory-based disease is far from complete. Moreover, the information about Cyps tissue distribution is unclear in the inflammatory process [6]. On the other hand, the modulation of Cyp is an interesting tool to figure out the relationship between inflammation and Cyps. The only commercial compound that modulates Cyps and inhibits their PPIase activity is the immunosuppressor cyclosporin A (CsA) and its analogues. CsA is frequently employed in transplantation and its use has been studied for myocardial ischemia–reperfusion injury treatment [20]. However, there is controversial information about its therapeutic use due to its toxicity and side effects [21]. This is related to the capacity of CsA to modulate several Cyps, including CypD [22]. Thus, the study of the modulation of Cyps is a useful tool to better understand the relationship of Cyps with inflammation.

To mimic low-grade systemic inflammation in humans, several animal models are well established. In this sense, the mouse model of inflammation induced by a high-fat diet (HFD)-induced is widely used to investigate inflammatory-related diseases and a variety of metabolic disorders, such as atherosclerosis or diabetes. HFD induces adipocyte inflammation, ROS production, and macrophage infiltration, leading to a low-grade systemic inflammatory response [23,24]. Therefore, this work aimed further investigate the pattern distribution of Cyps in an animal model of systemic inflammation. Hence, in this study, HFD-induced inflammation mice were used to determine CypA, CypB, CypC, CypD, and the CD147 receptor expression levels in the aorta, liver, and kidney and their association with the inflammatory process. Moreover, the effects of the modulation of CypA in this inflammatory model were also studied.

2. Material and methods

2.1. Chemicals and solutions

The synthetic compound, the GraA-derivative, was kindly donated by Dr. Romo group from the Department of Chemistry and Biochemistry, Baylor University, Texas, US. The GraA-derivative compound was named -(-) 23d or compound 1 in previous works [25–27].

Mouse High Sensitivity T Cell Magnetic Bead Panel Milliplex® map kit (#MHSTCMAG-70 K-07) and Polyvinylidene difluoride (PVDF) membrane were obtained by Merck (Madrid, Spain). The composition of phosphate buffer saline (PBS) solution used was (in millimolar) 137 ClNa, 8.2 Na2HPO4, 3.2 KCl, 1.5 KH2PO4, and 2 EDTA, pH 7.2–7.4. SuperSignal west pico and SuperSignal west femto were obtained from Thermo Fisher Scientific (Madrid, Spain). Anti-PPIA polyclonal antibody (cat. No. E-AB-15306, lot. DK0674), anti- PPIB polyclonal antibody (cat. E-AB-22123, lot. AC0235), and anti-PPIC polyclonal antibody (cat. E-AB-53088, lot. SG5377) were bought in Elasbscience (Madrid, Spain). Anti-CypD antibody (cat. No. ab64935, lot. GR51090-7), anti-CD147 antibody (cat. No. ab188190, lot. GR3250057), and Anti-GAPDH (cat. No. G8795, lot.) were from Abcam (Madrid, Spain). Polyacrylamide gels and molecular weight marker Precision Plus Protein Standards Kaleidoscope were obtained from Bio-Rad (Barcelona, Spain). Protease Inhibitor Complete Tablets and Phosphatase Inhibitor Cocktail Tablets were from Roche (Madrid, Spain). ImmPRESS® VR Anti-Mouse IgG HRP Polymer Detection Kit and BLOXALL were purchased from Vector Laboratories (Burlingame, CA, USA). Diaminobenzidine (DAB)-positive chromogen was from Dako (Glostrup, Denmark). Tekland global diet TD. 2018S and Tekland custom diet TD. 02028 were purchased in Envigo (Barcelona, Spain). The rest of the chemicals and reagents were obtained from Sigma-Aldrich (Madrid, Spain).

2.2. Experimental animals

In vivo studies were performed using 4-week-old female C57BL/6 mice obtained from Charles Rivers Laboratories (Barcelona, Spain). All animals were kept in the facilities of the animal care center of Universidad Santiago de Compostela under controlled temperature (24 °C), humidity (40–80%), and a light and dark cycle of 12 h. Water and food were provided *ad libidum*. All animal protocols employed were approved by the Institutional Animal Care Committee of the University of Santiago de Compostela under procedure number 06/19/LU-002, authorized on March 1, 2019 (A12X00509), and were performed following the Guide for the Care and Use of Laboratory Animals of the National Academy of Sciences (USA) and following the principles of European directives (EU directive 2010/63/EU) and Spanish legislation (Real Decreto 53/2013, Decreto 296/2008).

12 mice were randomly divided into 2 groups: group 1, controls fed with a standard diet (SD, Tekland global diet TD. 2018S, 5.5 % fat) (n = 6), and group 2, mice fed with a high-fat diet for 10 weeks (HFD; Tekland custom diet TD. 02028, 21.2 % fat and 1.25 % cholesterol) (n = 6).

To test the GraA-analogue, 18 mice were randomly divided into 3 groups: group 1, controls fed with SD (n = 6); group 2, mice fed with HFD (n = 6) and group 3, mice fed with HFD and injected intraperitoneally (IP) injected with GraA-analogue (n = 6). Mice were IP injected with the compound dissolved in saline solution (at 0.1 mg/kg) twice a week, for 10 weeks. Controls mice (groups 1 and 2) were IP injected with saline solution.

During experiments, animals were weighed biweekly. Euthanasia was performed on day 70 in a CO_2 chamber and tissue samples were collected for subsequent experiments. Serum was obtained from blood extracted by postmortem cardiac puncture and stored at –80 °C until analysis.

2.3. Histological evaluation

Aorta, liver, and kidney were collected for histological examination immediately after euthanasia. Samples were fixed in Bouin's solution and after 24 h were transferer to 70 % ethanol. Then, the specimens were embedded in paraffin wax and cut into serial transverse sections of 3 μm tick, mounted in slides, and dried overnight at 37 °C. Tissue sections were stained with hematoxylin and eosin (HE) for routine histological analyses, OMSB (Combined Orcein and Martius Scarlet Blue), or Gallego's trichrome for specific analyses [28,29].

For immunohistochemistry (IHC) studies, thin sections from paraffin-embedded samples of mice organs were placed onto slides treated with silane, to improve section adherence, and dried overnight at 37 °C. Endogenous peroxidase activity and non-specific binding were blocked by incubation with a peroxidase-blocking solution (BLOXALL). Then, the slides were incubated with the primary antibody (anti-CypA, anti-CypB, anti-CypC, anti-PPIF, or anti-CD147 antibodies) for 4 h. Three washes in PBS containing Tween-20 were done between all subsequent steps. Then, a commercial kit including a peroxidase (HRP)-labelled polymer conjugated to mouse/rabbit secondary antibody was used following the manufacturer's instructions. The detection of the peroxidase reaction was performed using DAB as the chromogen. For

this, DAB was diluted 1:50 with PBS-Tween and added to the slices for 1 min at room temperature. Finally, the samples were dehydrated through alcohols, cleared in xylene, and coverslipped with DePex mounting medium. Samples for which the primary antibody was omitted were used as negative controls. Digital images were captured with Olympus DP74 digital camera paired with an Olympus AX70 microscope.

2.4. Preparation of samples for Transmission Electron Microscope (TEM)

For TEM evaluation, aorta samples (1 mm3) were fixed by immersion in 2.5 % glutaraldehyde, at 4 °C for 24 h and rinsed thrice with 0.1 M with PBS. Then, specimens were postfixed by immersion in 1 % OsO4 in 0.1 M cacodylate trihydrate buffer for 1 h, then samples were rinsed and dehydrated in a graded ethanol solution, including one bath with 70 % ethanol and 0.5 % uranyl acetate, rinsed in propylene oxide, and embedded in Epon 812 (Momentive Specialty Chemicals Inc., Houston, TX, USA). To obtain ultrathin sections of samples, a Leica Ultracut UCT ultramicrotome was used (Leica Microsystems GmbH, Wetzlar, Germany), and they were counterstained with uranyl acetate and lead citrate. Ultrastructural analysis of 1 nm thick samples was performed with a JEOL JEM-1011 Transmission Electron Microscope (Jeol Ltd., Tokyo, Japan).

2.5. Determinations of interleukins

Levels of IFN-γ, IL-2, IL-6, IL-10, TNF-α, and MCP-1 were determined in mouse serum using a magnetic bead-based multiplex immunoassay (Milliplex® Map Kit) according to the manufacturer's instructions and as described in our previous work [14]. The median relative fluorescence units were measured using the Luminex® 200™ with xPONENT® software. All samples were run by duplicate and the concentrations were calculated using a standard curve. The range of determination was 0.49–2000 pg/mL for IFN-ϒ, 0.98–4000 pg/mL for IL-2, 0.98–4000 pg/mL for IL-6, 1.34–5500 pg/mL for IL-10, 3.91–16,000 pg/mL for MCP-1 and 0.49–2000 pg/mL for TNF-α. Serum levels below the lower limit of determination were undetectable and were considered as 0 pg/mL for statistical analysis. There was no or negligible cross-reactivity between the antibodies and any of the other analytes. The intra-assay coefficient of variation of the ELISA kits was <5%. The inter-assay coefficient of variation of the ELISA kits was <15%.

2.6. Western blot analysis

Western blot was performed to determine the expression of CypA, CypB, CypC, CypD, and CD147 receptor in the aorta, liver, and kidney lysates. 10 μg of total protein of organ lysates was used for electrophoresis. Samples for electrophoresis were resolved on 4–20% polyacrylamide gels and transferred onto PVDF membrane. To determine the protein size Precision Plus Protein Standards Kaleidoscope molecular weight marker was used. Afterward, membranes were blocked with 0.5% BSA diluted in wash buffer, and antibody incubation was performed using SNAP i.d. protein detection system. The immunoreactive bands were analysed using the Supersignal West Pico or Supersignal West Femto and the Diversity GeneSnap software (Syngene). CypA was detected with anti-CypA (1:2000), CypB was measured with anti-CypB (1:2000), CypC was analysed with anti-CypC antibody (1:2000), CypD was assessed with anti-PPIF (1:5000) and CD147 receptor with anti-CD147 antibody (1:5000). The signal was normalized by that of GAPDH (1:2000). The specificity of anti-CypA, anti-CypB, anti-CypC, and anti-CypD primary antibodies was checked. For this purpose, 0.25 μg of human recombinant Cyps A, B, C, and D proteins were loaded in polyacrylamide gels and followed the aforementioned protocol (Supplementary figure 10).

2.7. Statistical analysis

Results were expressed as mean ± SEM of a minimum of three experiments and were performed by duplicate or triplicate. Comparisons were analyzed using ANOVA statistical analysis followed by post hoc Dunnet's *t*-test. P values < 0.05 were considered statistically significant.

3. Results

To induce systemic inflammation in mice, 4-week-old female C57BL/6 mice were fed with HFD for 10 weeks. Mice fed with SD were used as a control. All mice were weighed weekly. At the beginning of the study, the mice weighed about 16 g. The weight of mice from HFD group was higher from the fifth week, compared to the control group. The average weight of mice from HFD group was 21.30 ± 0.33 g at week 10, meanwhile, the mice fed with SD weighed 20.64 ± 0.79 g. Although the mice that were fed with HFD weighed more than the controls, the difference was not significant.

Then, to check if HFD induces systemic inflammation in mice, the levels of inflammatory mediators were measured in serum at week 10. As shown in Fig. 1A, IFN-ϒ was 10 times higher in the HFD group than in the control ($p < 0.01$). Also, the serum levels of IL-2 and IL-6 were significantly enhanced in mice fed with HFD in comparison to controls (Fig. 1B-C; $p < 0.05$). Moreover, the anti-inflammatory mediator IL-10 was elevated in mice from the control group versus mice from HFD group (Fig. 1D; $p < 0.05$). In the case of MCP-1 and TNF-α levels were both doubled in the serum of HFD mice than in the serum of controls (Fig. 1E-F; $p < 0.001$). Therefore, the inflammatory mediators were significantly increased in response to HFD, resulting in systemic inflammation. In this sense, this is a proper inflammatory model.

After euthanasia, the mice were subjected to macroscopic observation at necropsy. Only hepatic alterations in the HFD-fed group were found. The liver of the control mice was smaller, with a smooth and shiny surface and typical color. Nevertheless, the liver from mice fed with HFD showed a rough surface, pale pink color, and hepatomegaly (Supplementary Fig. 1). These macroscopic findings were compatible with hepatic steatosis. Then, the aorta, liver, and kidney were recollected to study the levels and distribution of Cyps and the CD147 receptor upon inflammatory conditions. In addition, a histopathological study was performed on these organs to assess the effect of HFD-stimulated inflammation. These tissues were chosen based on their implication in inflammatory-based diseases and their relationship with Cyps [6]. The aorta was studied due to its role in vascular inflammation and inflammatory cardiovascular diseases, such as atherosclerosis [14,15]. The liver and the kidney were selected because they participate in systemic inflammation [30]. Subsequently, to investigate CypA, B, C, D, and the CD147 receptor expression levels in tissues, western blot analysis was performed. Firstly, as Fig. 2 shows, Cyps levels were measured in the aorta. In this regard, the expression ratio of CypA was significantly elevated in aortic tissues from the HFD group compared to controls (Fig. 2A, $p < 0.01$). CypB levels were the same in the aorta of both groups (Fig. 2B), however, CypC expression was almost doubled in the aortic tissues of HFD mice compared to SD mice (Fig. 2C; $p < 0.05$). The expression of CypD, as well as CypB, were the same in all mice studied (Fig. 2D). Nevertheless, the expression levels of CD147 were significantly higher in the aorta of HFD-fed mice than in controls (Fig. 2E, $p < 0.01$). Moreover, bivariate correlation analysis of serum proinflammatory cytokines, Cyps, and CD147 receptor revealed a significant correlation between CypA, CypC, and CD147 and proinflammatory cytokines ($p < 0.05$; Supplementary Table 1).

Then, Cyps levels were measured in the liver (Fig. 3). In this sense, the levels of CypA protein were significantly enhanced in HFD mice livers (Fig. 3A; $p < 0.05$). CypB levels remain unchanged in the HFD (Fig. 3B). In addition, the expression ratio of CypC was lower in the liver tissues of HFD mice compared to SD mice (Fig. 3C; $p < 0.001$). However, hepatic expression of CypD was significantly increased in mice fed with

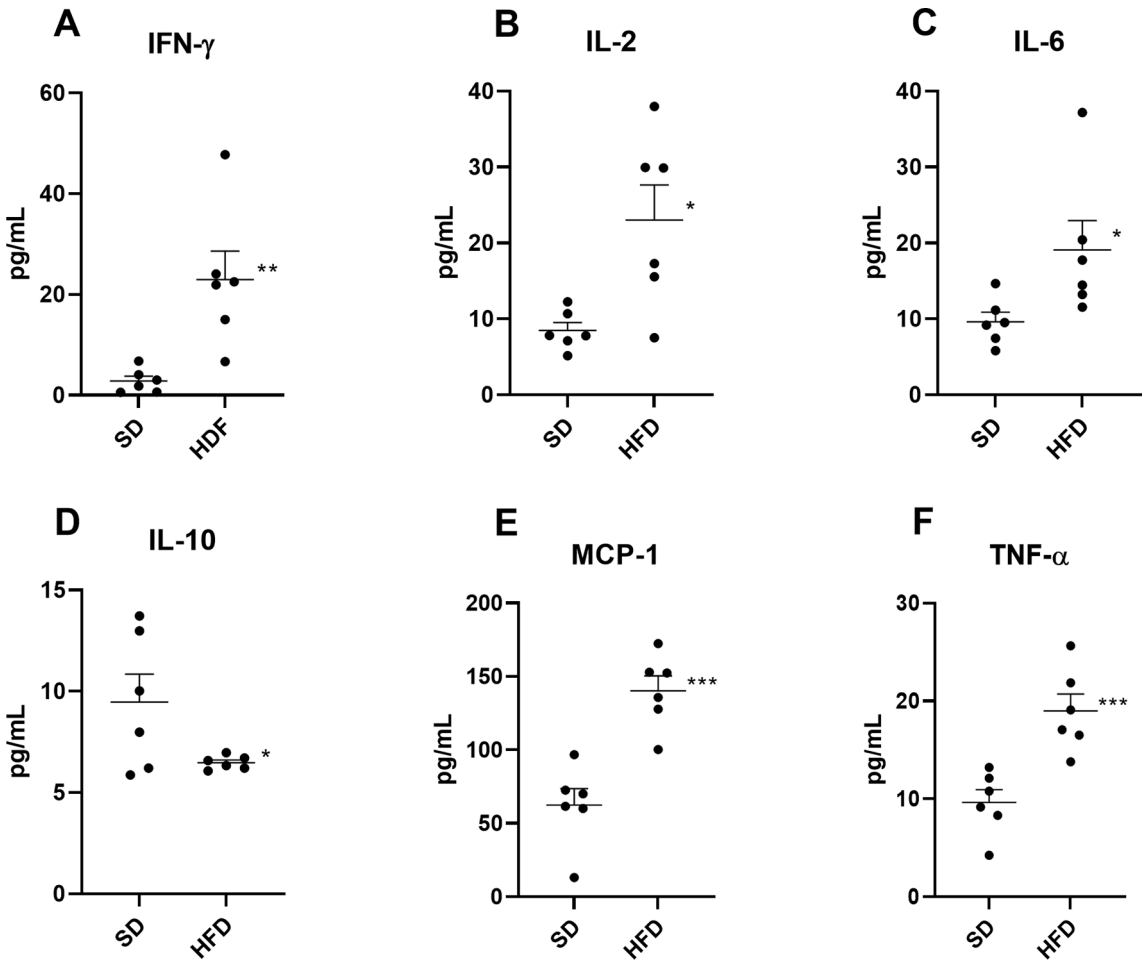


Fig. 1. Cytokine serum levels of SD and HFD-fed mice. IFN-ϒ (A), IL-2 (B), IL-6 (C), IL-10 (D), MCP-1 (E), and TNF-α (F) serum levels were measured by ELISA. Data are represented as dots of Ils levels in SD and HFD-fed mice plus mean ± SEM of N = 6 independent experiments performed by duplicate. The values are shown as the difference between serum from the SD group versus serum of the HFD-fed group by ANOVA statistical analysis followed by post hoc Dunnet's *t*-test. $^{*}p < 0.05$, $^{**}p < 0.01$, and $^{***}p < 0.001$. IFN-ϒ: interferon ϒ; IL: interleukin; MCP-1: monocyte chemoattractant protein-1 TNF-α: tumour necrosis factor α. HFD: high-fat diet; SD: SD: standard diet.

HFD than in controls (Fig. 3D; $p < 0.05$). Besides, the receptor CD147 was also significantly elevated in the liver of the HFD group (Fig. 3E; $p < 0.05$). Furthermore, there is a positive correlation between the levels of inflammatory mediators and the expression levels of CypA, CypD, and the CD147 receptor ($p < 0.05$; Supplementary Table 1). In the case of expression levels of CypC in the liver, the bivariate correlation analysis showed a negative correlation with the proinflammatory cytokine levels ($p < 0.05$). Moreover, the profile of Cyps in the aorta is different from the liver in terms of inflammation.

As Fig. 4 shows, Cyps expression levels were assessed in renal tissues. CypA and D protein levels remain unchanged in the kidney of the HFD-fed group compared to SD group (Fig. 4A and D). Moreover, the expression of CypB was higher in renal tissues from HFD-fed mice than in controls (Fig. 4B, $p < 0.05$). In the same way, CypC was also elevated in the kidney from the HFD group (Fig. 4C, $p < 0.05$). Furthermore, CD147 receptor expression was significantly enhanced in the kidney of HFD-fed mice (Fig. 4E, $p < 0.05$). In line with these results, the bivariate analysis revealed a positive correlation between CypB, CypC, CD147, and the serum levels of cytokines ($p < 0.05$; Supplementary Table 1). Therefore, there is a clear distinct pattern of Cyps levels alteration in each organ under inflammatory conditions.

Afterward, given the changes found in CypA, B, C, D, and the CD147 receptor expression levels, their tissue distribution was studied using IHC analysis. Therefore, a histological examination of tissues was first performed. Primary microscopical features of the aorta were studied in cross-sections stained with HE. As shown in Fig. 5, endothelial cells (ECs) and smooth muscle cells (black arrow Fig. 5B) of the aorta exhibited a normal shape in both control and HFD-fed mice (Fig. 5A–D). Furthermore, the elastic layers (Fig. 5F, black arrow) were clear and arranged in order. Hence, Gallego's Trichome or OSMB staining techniques were used to deepen the study of the primary microscopic characteristics of the aorta (Fig. 5E–L). These stains confirm that the aorta of all mice shows regular structural features. However, there is an increased lipid accumulation in the adipose tissue (AT, Fig. 5C–G) from mice fed with HFD. Thus, the ultrastructure of these blood vessels was further studied by employing transmission electron microscopy (TEM). After TEM analysis, a standard structure of the aorta with continuous elastic fibres was observed in control animals (Fig. 5M and 5 N) and some changes in the aortic wall from HFD were evident (Fig. 5O–R). In this sense, TEM displays some alterations in matrix architecture in the aorta from mice fed with HFD. Several subendothelial spaces and clefts within the endothelium were observed (arrows; Fig. 5P and R). Besides, a density reduction was evident in some elastic fibres from HFD mice (asterisks; Fig. 5O and R). The elastin lamellae were discontinuous in various areas of the aorta of HFD group evidencing a shearing between layers and cell infiltration (Fig. 5R). The cytoplasm of a few vascular smooth muscle cells (VSMCs) contained lipid droplets and lysosomes of different sizes (arrowhead; Fig. 5O and Q). Furthermore, nuclear chromatin condensation and karyolysis were observed in some VSMCs (Fig. 5O and Q). A vacuolated VSMCs showed foam cell-like features

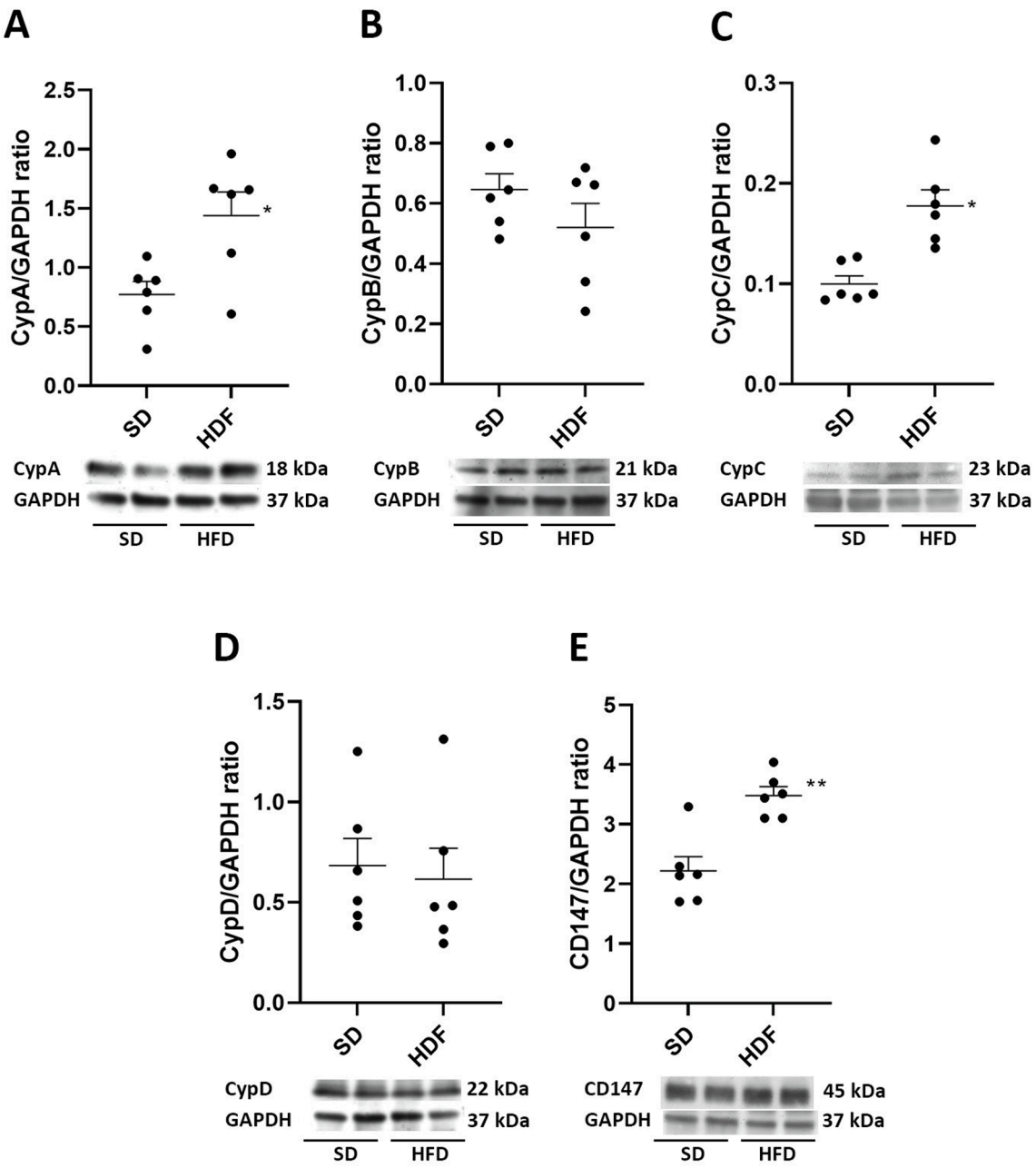


Fig. 2. CypA, B, C, D, and CD147 receptor expression levels in aorta from SD and HFD-fed mice. CypA (A), CypB (B), CypC (C), CypD (D), and CD147 (E) expression levels were measured by western blot on aortic lysates. The protein expression was determined by the ratio of the sample value to internal standard control (GAPDH). One representative Western blot is shown. Data are the result of average ± SEM of a minimum of N = 6 independent experiments performed by duplicate. The values are shown as the difference between the aorta of SD and HFD-fed mice, $*p < 0.05$ and $**p < 0.01$. One-way ANOVA test with Dunnet's post hoc analysis and Students *t*-test were used for statistical analysis. CypA: cyclophilin A; CypB: cyclophilin B; CypC: cyclophilin C; CypD: cyclophilin D; HFD: high-fat diet; SD: SD: standard diet.

(Fig. 5Q). This cell was characterized by plenty of lipid droplets within the cytoplasm surrounded by elastic and collagen fibres. In addition, some collagen fibre abnormalities are evident in the aorta of HFD animals (Fig. 5O). All these features are compatible with a very early atherogenesis stage and vascular inflammation [31,32]. These findings show that this model of systemic inflammation is also valid for vascular inflammation.

Then, the tissue distribution of Cyps and their receptor were studied by IHC. Thus, vascular cross-sections of the aorta were immunostained with anti-CypA, CypB, CypC, CypD, or CD147. As Fig. 6 shows, the CypA, B, C, and D markers stained the VSMCs and ECs cytoplasm and some structures of the tunica adventitia, like collagen fibres (Fig. 6C-F). However, the immunolabelling intensity of Cyps seems to be the same in the aorta from both groups. Besides, the CD147 marker stained the surface of cells from the tunica adventitia and adipocytes from adipose tissue (AT, Fig. 6G and 6H). Furthermore, the anti-CD147 staining reflected a high level of CD147 expression in aortic sections from the HFD group (asterisk, Fig. 6H). Nevertheless, the distribution of Cyps and CD147 within the artery wall seems to be the same in SD and HFD-fed mice.

In the histopathological study of the liver, the hepatic sections were stained with HE as shown in Fig. 7. The liver parenchyma from control mice shows a regular structure (Fig. 7A). Meanwhile, as Fig. 7B shows, hepatocytes from the liver of HFD-fed animals showed cellular swelling

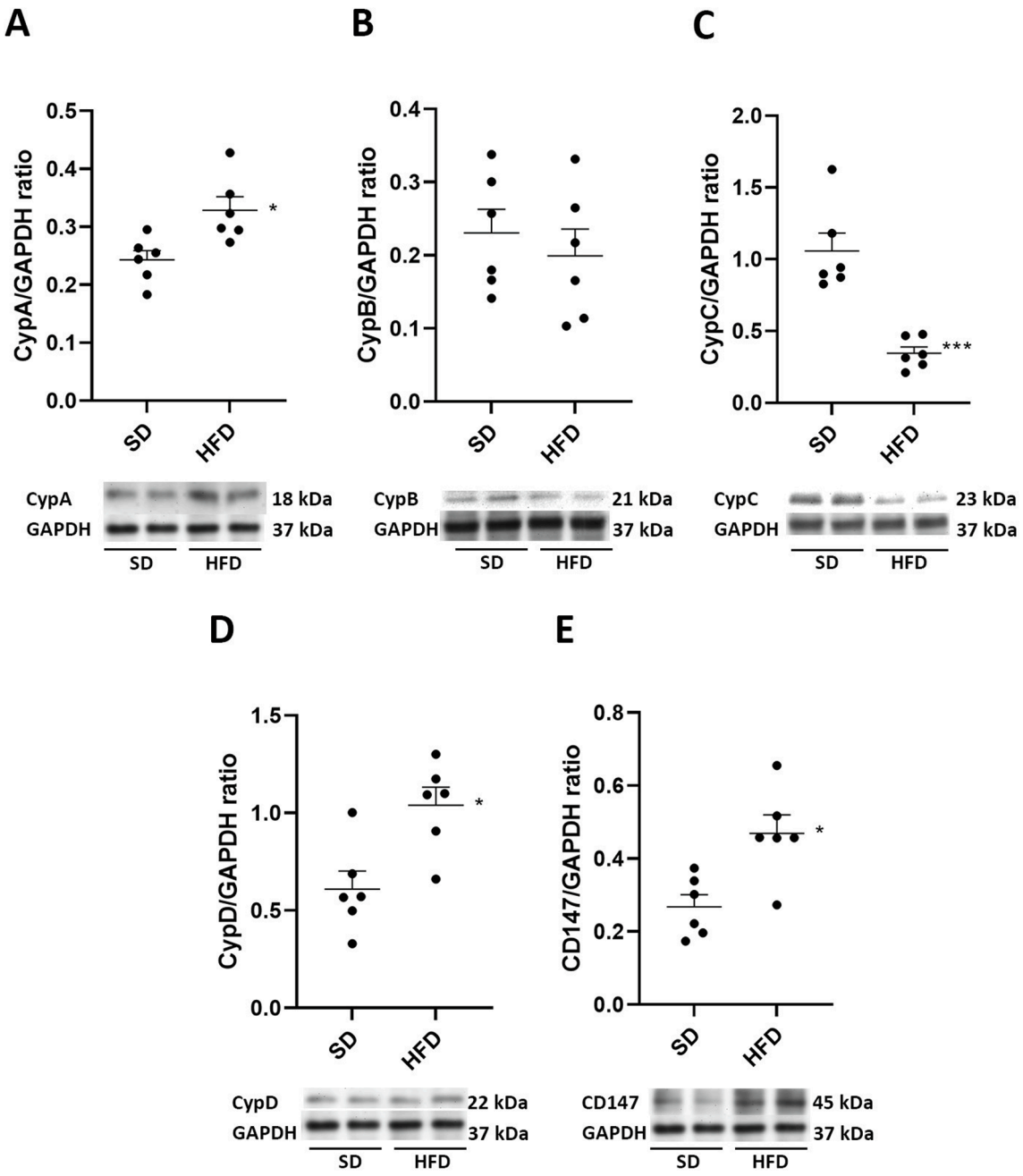


Fig. 3. CypA, B, C, D, and CD147 receptor expression levels on the liver from SD and HFD-fed mice. CypA (A), CypB (B), CypC (C), CypD (D), and CD147 (E) expression levels were measured by western blot on liver lysates. The protein expression was determined by the ratio of the sample value to internal standard control (GAPDH). One representative Western blot is shown. Data are the result of average ± SEM of a minimum of N = 6 independent experiments performed by duplicate. The values are shown as the difference between the liver from SD and HFD-fed mice, $*p < 0.05$ and $***p < 0.001$. One-way ANOVA test with Dunnet's post hoc analysis and Studenťs *t*-test were used for statistical analysis. CypA: cyclophilin A; CypB: cyclophilin B; CypC: cyclophilin C; CypD: cyclophilin D; HFD: high-fat diet; SD: SD: standard diet.

(asterisks, Fig. 7B) with lipid vacuoles of different sizes within the cytoplasm (arrow, Fig. 7B). Macrovesicular steatosis was mainly found in the periportal area and microvesicular steatosis was in the centrilobular area. These findings confirm the hepatic steatosis found macroscopically in the necropsy. Also, immune cell infiltrates were found in the lumen of hepatic sinusoids, being compatible with an inflammatory reaction (arrowheads). Then, tissue distribution of Cyps and CD147 receptor markers were assessed. IHC results show that CypA marker stained the cells within the hepatic sinusoids in the liver, however, liver sections of HFD mice contained several CypA-stained hepatocytes (arrows; Fig. 7C and 7D). CypB, C, and D also stained the cells within the hepatic sinusoids in the liver (Fig. 7E–J). In addition, some CypB-stained hepatocytes were found in the liver of SD mice (Fig. 7E). Furthermore, the anti-CD147 marker stained the surface of hepatocytes and hepatic sinusoids. However, the distribution of CypC, CypD, and CD147 within the artery wall seems to be the same in both mice groups.

Finally, the histopathological findings and Cyps tissue distribution were investigated in the kidney. Then, primary microscopical features of HE-stained renal cortex sections were studied. As Fig. 8 shows, the kidney sections of SD and HFD-fed mice showed regular structure, with regular renal glomerulus (arrow) and tubules (arrowhead; Fig. 8A and B). Subsequently, the tissue pattern distribution of Cyps in kidneys was

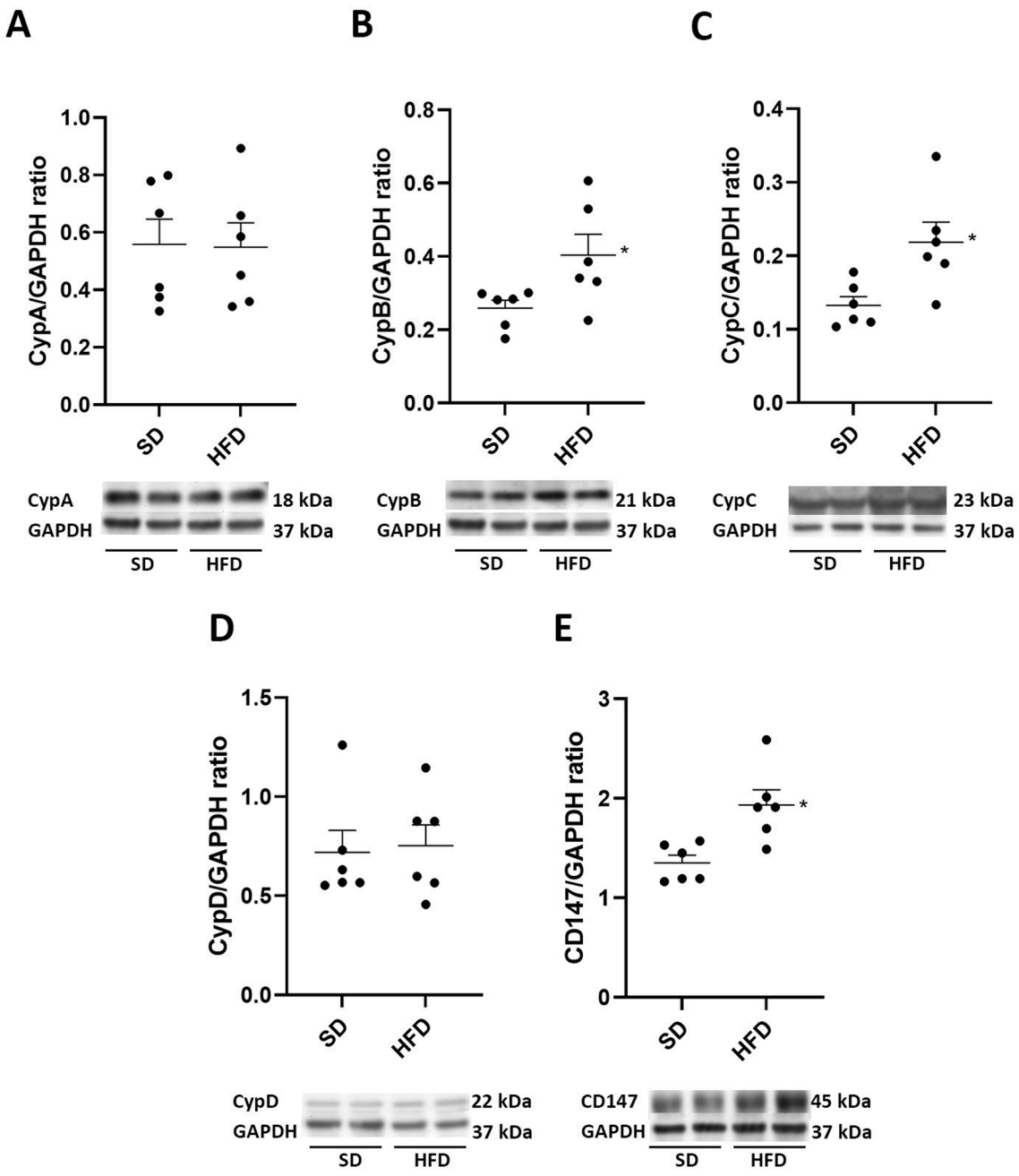


Fig. 4. CypA, B, C, D, and CD147 receptor expression levels on the kidney from SD and HFD-fed mice. CypA (A), CypB (B), CypC (C), CypD (D), and CD147 (E) expression levels were measured by western blot on kidney lysates. The protein expression was determined by the ratio of the sample value to internal standard control (GAPDH). One representative Western blot is shown. Data are the result of average ± SEM of a minimum of N = 6 independent experiments performed by duplicate. The values are shown as the difference between the kidney from SD and HFD-fed mice, $^*p < 0.05$. One-way ANOVA test with Dunnet's post hoc analysis and Student́s *t*-test were used for statistical analysis. CypA: cyclophilin A; CypB: cyclophilin B; CypC: cyclophilin C; CypD: cyclophilin D; HFD: high-fat diet; SD: SD: standard diet.

studied by IHC. Renal sections of SD mice showed several CypA, B, and C-stained tubules (arrowhead; Fig. 8C). Meanwhile, in kidneys from HFD mice, the glomeruli are also stained with CypA, B, and C (arrow; Fig. 8D). In the case of CypD, immunolabeling is present in both tubules and glomeruli from all kidneys (Fig. 8I and J). Moreover, the D147 is present on the surface of renal tubular epithelial cells and the immunolabelling of CD147 seems to be stronger in the kidney of HFD-fed mice than in controls (Fig. 8G and 8H).

Subsequently, to further explore the relationship between Cyps and inflammation, a CypA inhibitor, the GraA-derivative compound, was tested in the animal model of HFD-induced inflammation. This compound showed binding affinity towards CypA, inhibits calcineurin phosphatase activity, reduces IL-2 liberation, and reduces the inflammatory response in cells [25–27]. Therefore, mice were divided into 3 groups: SD-fed group, HFD-fed group, and HFD-fed and GraA-derivative treated group. In this sense, HFD-fed mice were IP injected with the synthetic GraA-derivative for 10 weeks. Then the inflammatory mediators were measured. The choice of this compound was based on its anti-inflammatory and antioxidant properties shown in previous studies [25–27]. Also, the IP route was chosen based on prior data [33]. Therefore, after 10 weeks of the experiment, as Fig. 9 shows, cytokine serum levels were measured. The IFN-ϒ and IL-2 serum levels were

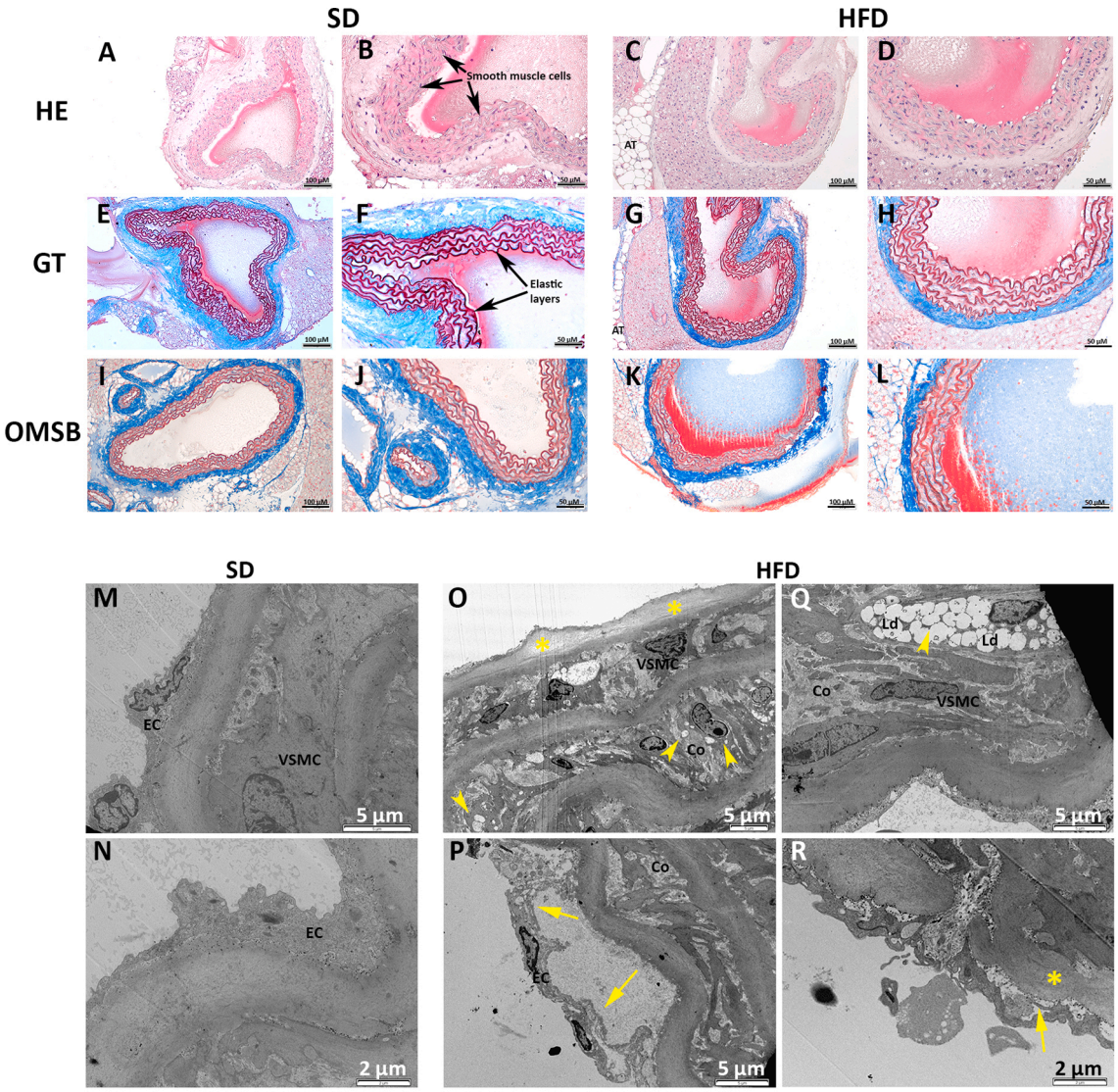


Fig. 5. Representative microphotographs of hematoxylin and eosin-stained cross-sections of aortic of SD and HFD-fed mice (A-L). Transmission Electron Microscopy of cross-sections of aortic of SD and HFD-fed mice (M—R). Scale bars, 100 µm, 50 µm, 5 µm and 2 µm. AT: adipose tissue; Co: collagen; EC: endothelial cells; Ld: lipid droplets; VSMCs: vascular smooth muscle cells.

significantly reduced in mice treated with the GraA-derivative compared with HFD-fed mice (Fig. 9A and B; $p < 0.05$). However, the serum concentration of IL-6 remains unchanged in treated mice, compared with mice from the HFD group (Fig. 9C). The levels of the anti-inflammatory IL-10 were elevated in mice after the treatment with the GraA-derivative compared with mice fed with HFD (Fig. 9D; $p < 0.05$). Furthermore, TNF-α and MCP-1 were both lower in the serum of treated mice than in HFD-fed mice (Fig. 9E and F; $p < 0.05$). Therefore, the systemic inflammation induced by HFD was reduced when CypA was inhibited.

Then, it was studied whether CypA and CD147 receptor tissue expression was affected by CypA inhibition. Therefore, the expression levels of CypA and CD147 were measured in the aorta and liver tissues. These organs were chosen because upon inflammatory conditions the expression of CypA and the receptor were increased. As Fig. 10 shows, the CypA expression was reduced up to control levels in the aorta of mice treated with the GraA-derivative (Fig. 10A; $p < 0.05$). Moreover, the expression of the CD147 receptor was also reduced in the aorta after 10 weeks of treatment (Fig. 10B; $p < 0.05$). Furthermore, CypA expression levels were significantly reduced in the liver of treated mice compared to HFD-fed mice (Fig. 10C; $p < 0.05$). Although the GraA-derivative also decreased the CD147 receptor in the liver, the reduction was not significant compared to the hepatic levels of the HFD group (Fig. 10D). Therefore, the CypA and CD147 levels were reduced in the aorta and liver when CypA was modulated.

4. Discussion

In the present work, a mouse model of inflammation was used to study the tissue distribution of Cyps and CD147 receptor levels. Therefore, to induce systemic inflammation, mice were fed with HFD (21.2 % fat and 1.25 % cholesterol) for 10 weeks [23]. Elevated levels of the pro-inflammatory cytokines IL-2, IL-6, TNF-a, and IFN-g and the chemokine MCP-1 were found in the serum of HFD-fed mice. These mediators are involved in several inflammatory diseases [34]. In addition, the main cytokine implicated in the suppression of the inflammatory response, IL-10, was found in lower concentrations in the serum of HFD group. Thus, increased levels of circulating proinflammatory mediators suggest that HFD-fed mice manifest a systemic inflammatory state. Consequently, this is a suitable model of inflammation and therefore a useful tool to study tissue levels of Cyps and its receptor. In this inflammatory model, increased levels of CypA, CypC, and CD147 were found in the aorta upon

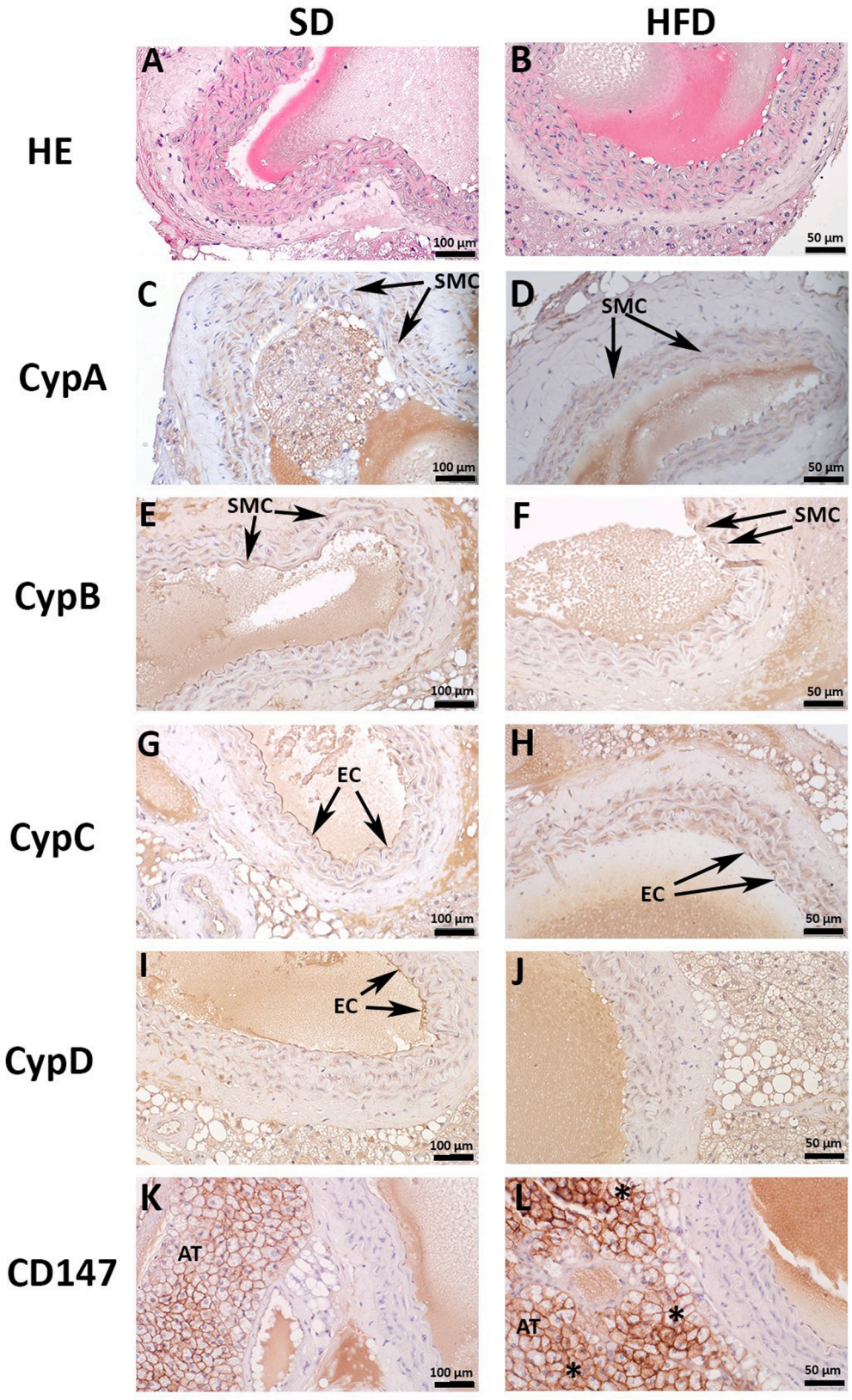


Fig. 6. Representative microphotographs of hematoxylin and eosin-stained cross-sections of aortic of SD and HFD-fed mice (A and B) and Immunohistochemical staining of CypA, CypB, CypC, CypD, and CD147 antibody (C-L). Scale bars, 100 μm, and 50 μm. AT: adipose tissue; CypA: cyclophilin A; CypB: cyclophilin B; CypC: cyclophilin C; CypD: cyclophilin D; EC: endothelial cells; HFD: high-fat diet; SD: SD: standard diet; SMC: smooth muscle cells.

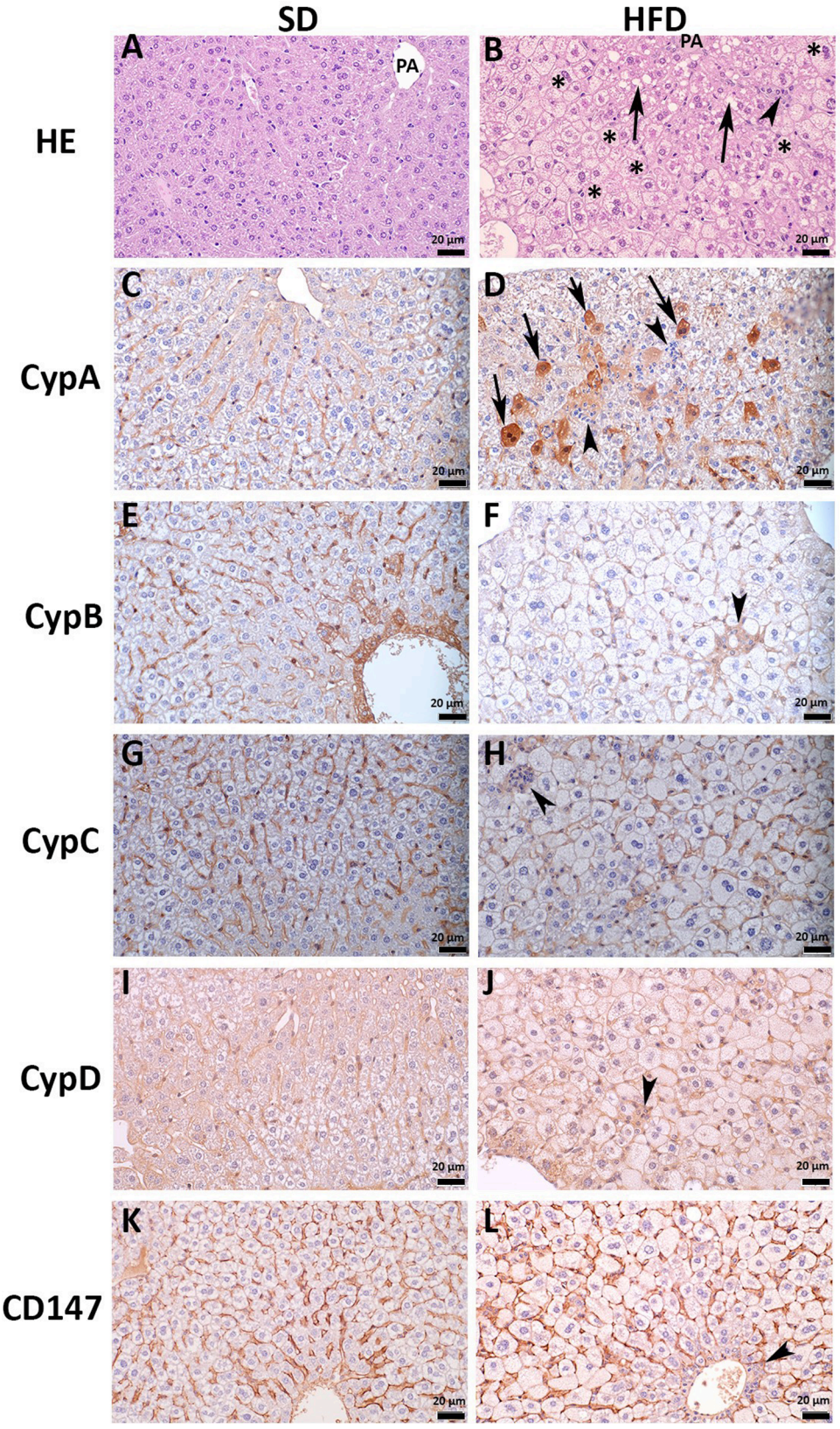


Fig. 7. Representative microphotographs of hematoxylin and eosin-stained liver of SD and HFD-fed mice (A and B) and Immunohistochemical staining of CypA, CypB, CypC, CypD, and CD147 antibody (C-L). Scale bars, 100 µm, and 50 µm. CypA: cyclophilin A; CypB: cyclophilin B; CypC: cyclophilin C; CypD: cyclophilin D; HFD: high-fat diet; PA: portal area; SD: SD: standard diet.

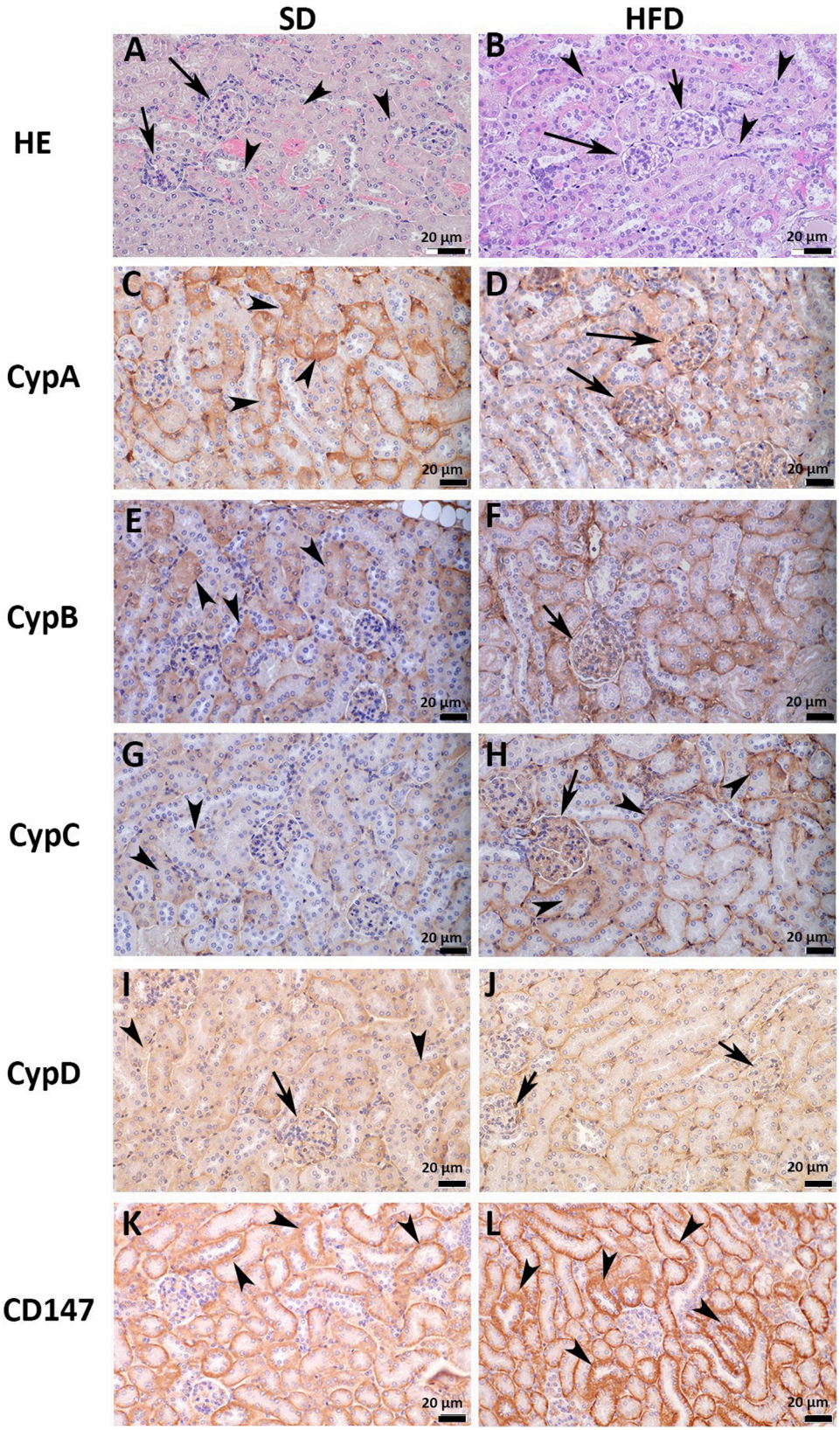


Fig. 8. Representative microphotographs of hematoxylin and eosin-stained renal cortex sections of SD and HFD-fed mice (A and B) and Immunohistochemical staining of CypA, CypB, CypC, CypD, and CD147 antibody (C–H). Scale bars, 100 μm, and 50 μm. CypA: cyclophilin A; CypB: cyclophilin B; CypC: cyclophilin C; CypD: cyclophilin D; HFD: high-fat diet; SD: SD: standard diet.

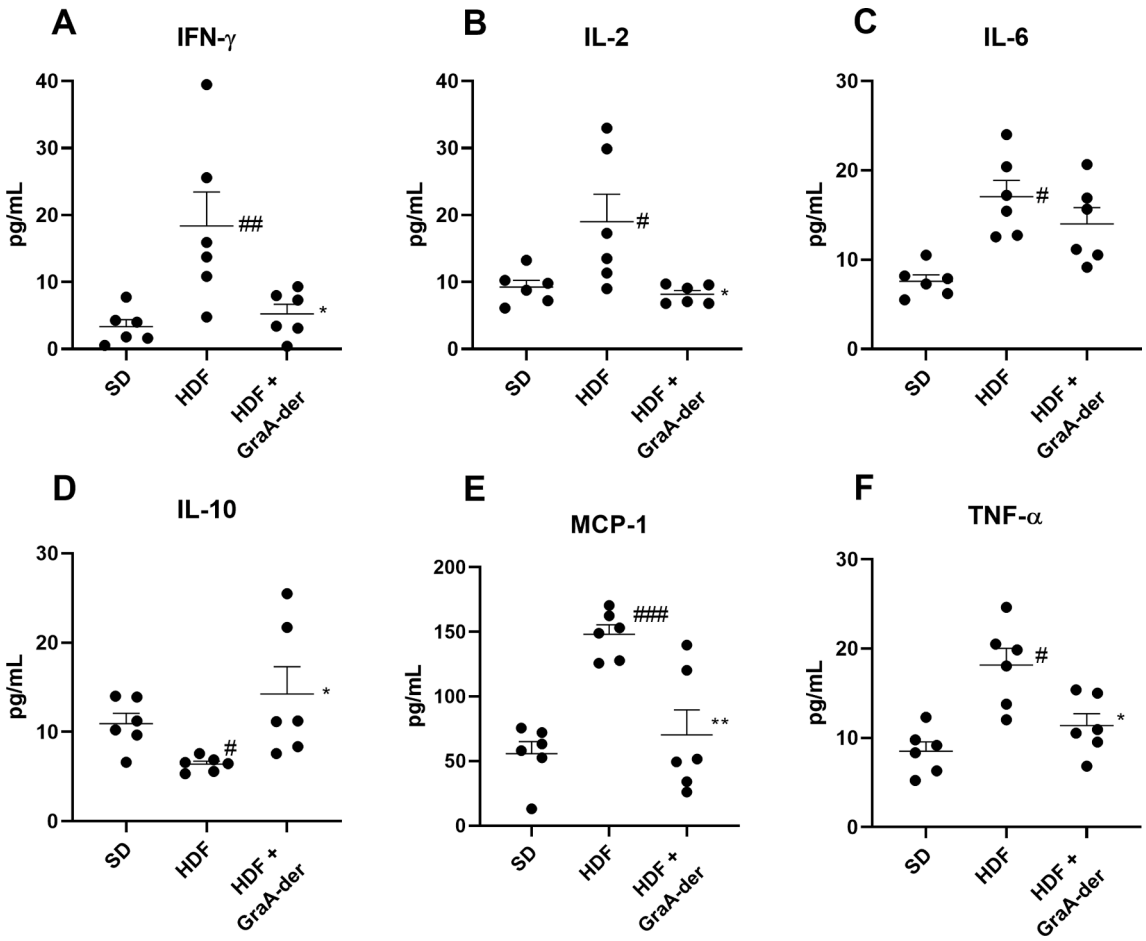


Fig. 9. Cytokine serum levels of SD-fed mice, HFD-fed mice, and HFD-fed mice treated with GraA-derivative. IFN-ϒ (A), IL-2 (B), IL-6 (C), IL-10 (D), MCP-1 (E), and TNF-α (F) serum levels were measured by ELISA. Data are represented as dots of Ils levels in SD, HFD-fed mice, and HFD-fed mice treated with GraA-derivative plus mean ± SEM of N = 6 independent experiments performed by duplicate. The values are shown as the difference between serum from the SD group versus serum from the HFD-fed group #p < 0.05, ##p < 0.01 and ###$p < 0.001$, or between serum from the HFD-fed group versus serum from the HFD-fed group treated with GraA-derivative by ANOVA statistical analysis followed by post hoc Dunnet's *t*-test. *$p < 0.05$ and **$p < 0.01$. GraA-der: gacilin A-derivative; IFN-ϒ: interferon ϒ; IL: interleukin; MCP-1: monocyte chemoattractant protein-1 TNF-α: tumour necrosis factor α; HFD: high-fat diet; SD: SD: standard diet.

inflammatory conditions. In the liver of HFD-fed mice, CypA, CypD, and CD147 expression levels were elevated, meanwhile, CypB and CypC were downregulated. Furthermore, CypB, CypC, and CD147 protein levels were augmented in the kidney. It is important to highlight that despite the several existing studies demonstrating the damage effects of HFD on mice tissues, it is the first time that Cyps and CD147 receptor profile was described in the kidney of the HFD-induced inflammation model [35,36]. In addition, to our knowledge, no prior study has measured CypB, CypC, CypD, and CD147 receptor levels in the aorta in inflammatory conditions. Moreover, there is a positive correlation between inflammatory mediators and Cyps expression levels in tissues. In addition, a negative correlation is observed between CypC in the liver and the inflammatory mediators. Therefore, there is a direct correlation between the degree of inflammation and the levels of specific cyclophilin in each tissue.

As aforementioned, the mice fed with HFD show signs of aortic injuries compatible with an early stage of atherosclerosis [32]. Moreover, collagen aberrations and abnormalities in ECs were found. These cells are involved in the inflammatory response and vascular diseases. They regulate leucocyte extravasation and cytokine production, among others. Under normal conditions, ECs and VSMCs from vascular walls remain quiescent [37]. However, upon inflammatory stimuli or oxidative stress, these cells are activated and release CypA. Moreover, the extracellular CypA, in turn, stimulates ECs and VSMCs activation, which aggravates the inflammation. Furthermore, it was demonstrated that CypA contributes to the progression of vascular lesions in high glucose conditions through the induction of foam-cell formation and increasing oxidative stress status [38]. In addition, extracellular CypA induces the production of pro-inflammatory cytokines via CD147 interaction [19]. In this sense, in the present study high levels of CypA in the aorta of mice with HFD-induced inflammation could be the cause of lesions in the aortic wall. Furthermore, this immunophilin could be promoting the production of proinflammatory mediators. Intracellularly, CypB is an ER-residing protein and participates in protein folding and trafficking. Besides, a second major role for CypB is to catalyse *cis-to-trans* isomerization of proline residues which is essential for proper collagen folding [39]. Although the aim of the present study was not to investigate intracellular levels of CypB, collagen fibre abnormalities found in the aorta of the HFD group could be mediated by intracellular CypB. In addition, there is a clear relationship between CypC and CVDs. Recently, our group has shown that extracellular CypC also induces ECs dysfunction [40]. Moreover, we have found elevated CypC levels in the serum of acute and chronic CAD patients [14,15]. These data are reinforced in the present study, where increased CypC levels were found in the aorta of HFD-fed mice. In this sense, high CypA and C levels could be promoting inflammation and vascular lesions compatible with an early stage of atherosclerosis.

In the present work, high lipid accumulation, compatible with hepatic steatosis, was observed in the liver of mice fed with HFD. Moreover, overexpression of hepatic CypA and D levels were found. CypA, in

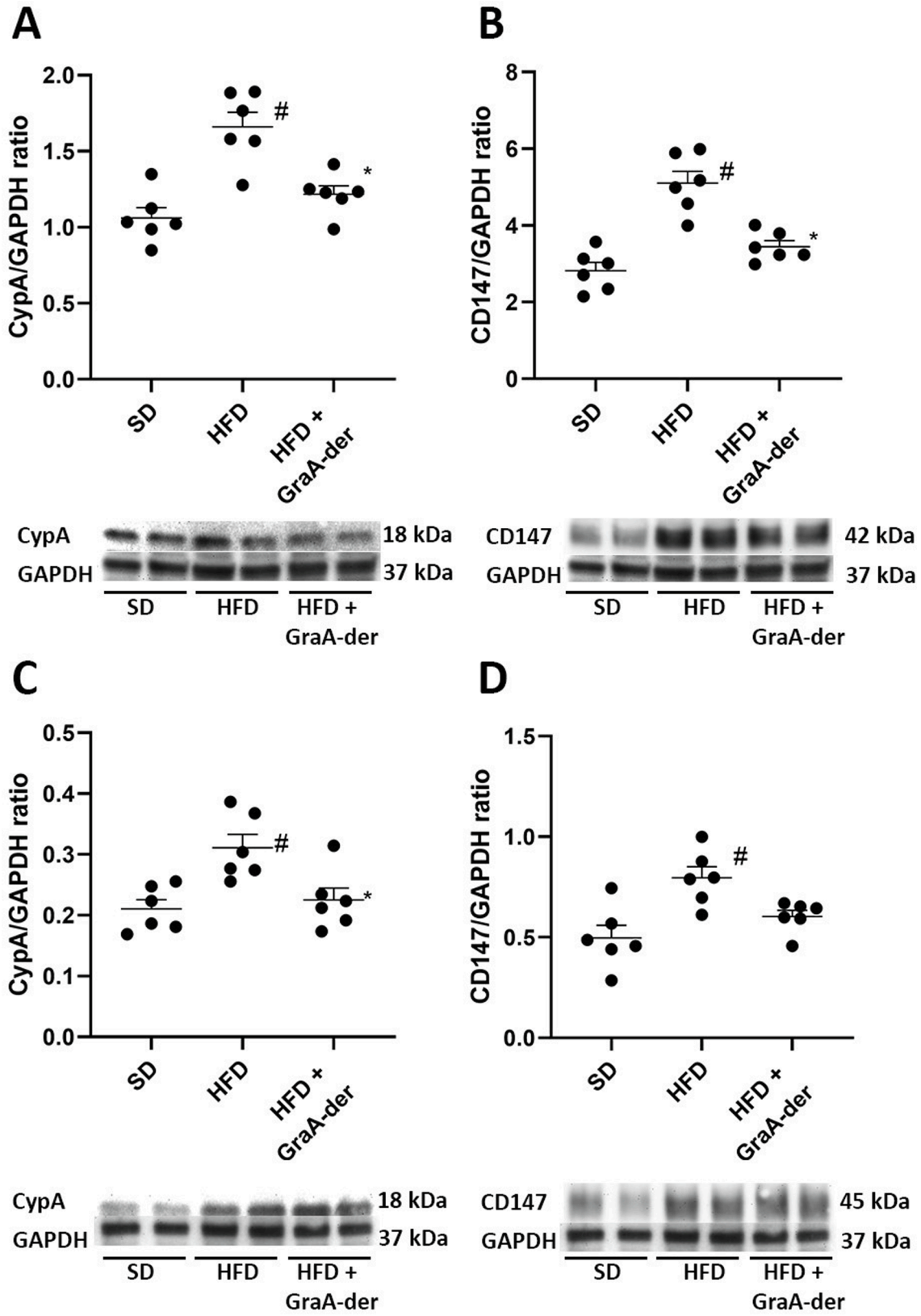


Fig. 10. CypA and CD147 receptor expression levels on the aorta and liver from SD-fed mice, HFD-fed mice, and HFD-fed mice treated with GraA-derivative. CypA (A) and CD147 (B) expression levels were measured on aorta tissue lysates, CypA (C) and CD147 (D) expression levels were measured on liver tissue lysates. The protein expression was determined by the ratio of the sample value to internal standard control (GAPDH). One representative Western blot is shown. Data are the result of average ± SEM of a minimum of N = 6 independent experiments performed by duplicate. The values are shown as the difference between SD group versus HFD-fed group, $\#p < 0.05$ and $\#\#p < 0.01$, or between HFD-fed mice group and the HFD-fed group treated with GraA-derivative by ANOVA statistical analysis followed by post hoc Dunnet's *t*-test, $*p < 0.05$. CypA: cyclophilin A; CypB: cyclophilin B; CypC: cyclophilin C; CypD: cyclophilin D; GraA-der: gracillin A-derivative; HFD: high-fat diet; SD: SD: standard diet.

addition to contributing to the inflammatory response, is believed to be involved in hepatic lipid accumulation. In this sense, it has been demonstrated that the genetic knockout of CypA reduces fat mass and adipocyte size in mice [41]. The cyclophilin isoform CypD also contributes to hepatic steatosis, as it is involved in fatty acid β-oxidation and glycolysis in the liver. It has been demonstrated that CypD deletion ameliorated hepatic steatosis and avoid weight induced by an HFD [42]. Furthermore, the overexpression of CypD preceded the accumulation of triglycerides in the liver and the development of hepatosteatosis [43]. Consequently, in the present study, hepatic steatosis could be due to increased hepatic levels of CypA and CypD, which may be contributing to systemic inflammation. Nevertheless, hepatic steatosis not only affects the mitochondria but also the primary organelle implicated in lipid synthesis, the ER. In this sense, the perturbation of lipid synthesis leads to ER stress and can induce unfolded protein response [44]. In addition to CypB, CypC is also an ER-resident cyclophilin and it could be secreted upon various stimuli. Intracellularly, CypB, and C are essential in ER stress response. Furthermore, the deletion of CypB and C induces dysregulation of ER redox homeostasis, ER stress, ROS production, and unfolded protein response [9]. We have observed decreased levels of CypB and C in the liver of HFD-fed mice. The slight concentration of these immunophilins in the liver could be inducing oxidative stress and participating in inflammatory state development. However, the role of CypB and C and their possible release from the liver during the inflammatory process and hepatic steatosis should be further studied. In addition, Cyps levels are differently altered in the aorta and liver, evidencing a distinct role for Cyps in each organ in the context of inflammation.

Consistent with previous reports, renal lipid build-up causes lipotoxicity leading to kidney injury. Moreover, the oxidative stress caused by systemic inflammation induces mitochondrial dysfunction [45]. CypA plays an important role in the pathogenesis of several kidney diseases, especially by attracting immune cells and promoting inflammation [46]. In this sense, high CypA serum levels have been found in patients with impaired kidney function and CAD [47]. Besides, in a model of acute kidney injury, CypA liberation was demonstrated, nevertheless, the intracellular levels of CypA remained unchanged in renal cells [48]. These data are in line with the results of the present study, where CypA expression was the same in the kidney of both SD and HFD-fed groups. Currently, there is controversial information about the pathophysiology of renal CypB. This immunophilin is crucial for the Na/K-ATPase pump location and activity in the human kidney [49]. Moreover, CypB has a protective role against aldosterone-induced oxidative stress, ER stress, and tubular cell injury. Nevertheless, overexpression of CypB has been found in the kidney of hypertensive rats, evidencing a cellular stress response in the renal epithelium [50]. In the case of CypC, it was first described in the kidney, however, little information about its renal function is available [6,10]. In the present paper, increased CypB and C levels in kidney tissues were detected in mice fed with HFD. Therefore, it could be hypothesized that renal CypB and C are implicated in the systemic inflammatory process. Also, the renal functions of Cyps are different from those of the aorta and liver.

Finally, CD147 receptor is a membrane-bound glycoprotein and is a signalling receptor for extracellular Cyps. This receptor mediates the pro-inflammatory activities of extracellular cyclophilins being essential for Cyps-mediated signal events [16–18]. Furthermore, CD147 mediates the chemotaxis activity of Cyps toward immune cells. In this sense, the CD147 overexpression enhances the chemotaxis of leucocytes, magnifying the inflammatory response. Besides, it is implicated in the pathogenesis of several diseases [18,51]. Also, the interaction of CypA/CD147 promotes cytokine storm through the Nuclear Factor kappa B pathway and extracellular regulated protein kinase 1/2 signalling pathways [52]. In the current study, elevated expression of CD147 has been detected in the aorta, liver, and kidney of mice fed with HFD. Furthermore, CypA, through CD147 binding, induces foam cell formation and ROS generation, being a modulator of vascular inflammation [53]. So, foam cells found in the aorta in the present work might be associated with the overexpression of CypA and CD147 receptor. In addition, high levels of CypC in the artery wall could also be related to these processes. On the other hand, overexpression of CD147 is associated with hepatic steatosis, acute kidney injury, and renal fibrosis development autophagy in mice fed with HFD [54,55]. Consequently, it could be hypothesized, from our results, that Cyps through their binding to the CD147 receptor are involved in these processes.

Among all Cyps previously described, CypA has been the most studied and the one with the clearest role in the pathophysiology of inflammation [6]. Therefore, the modulation of CypA is useful to better understand the relationship between inflammation and Cyps. In this sense, the well-known immunosuppressive CsA was used in several studies to modulate CypA. However, CsA is not specific for CypA since it also modulates other Cyps such as CypB and D [22]. Moreover, its use *in vivo* is being reduced because it causes nephrotoxicity, and it has been associated with diabetes and hypertension [56]. Therefore, in the present work, the synthetic compound GraA-derivative, a CypA modulator, was used [25]. The GraA-derivative showed kinetic equilibrium dissociation constants value in the nanomolar range for CypA and no union for CypD [25]. Furthermore, this compound inhibits the calcineurin phosphatase activity and decreases pro-inflammatory mediators' liberation and the translocation of pro-inflammatory proteins *in vitro* [25–27]. In the present work, serum levels of pro-inflammatory proteins were reduced in HFD-fed mice after 10 weeks of GraA-derivative treatment. Knowing the implication of CypA in the cytokine storm activation, it could be hypothesized that inflammatory response is reduced when CypA is modulated with the compound [52]. Moreover, the CypA expression levels were also downregulated in the aorta and liver of mice from the HFD group. The beneficial *in vitro* role of Cyps inhibition has also been reported in the development of non-alcoholic steatohepatitis and hepatocellular carcinoma [57]. Moreover, Cyps inhibitors have shown good results in patients with non-alcoholic steatohepatitis in a phase 2b study [58]. Furthermore, this compound also leads to the reduction of the CD174 receptor expression. Knowing that extracellular Cyps need to bind to the CD147 receptor to exert their inflammatory activity, the extracellular functions of CypB and CypC could also be inhibited when CypA is modulated [12]. Also, this compound could have binding affinities toward CypB or C. Furthermore, the activity shown by the compound may also be due to its potential to inhibit calcineurin phosphatase activity through CypA modulation. In this sense, the inhibition of calcineurin activity was widely associated with CypA. When CypA forms a complex with a drug, such as CsA, calcineurin activity is inhibited [59,60].

Taken together, all these data strengthen the relationship between Cyps, CD147 receptor, and inflammation. Furthermore, these findings suggest that the tissue distribution of each Cyp is not alike, and they have different pattern distributions in each organ in the context of inflammation. Moreover, CypA modulation reduces the inflammatory response. However, there are still relevant questions about the role of Cyps in inflammation. In this sense, the critical site of cyclophilin release remains unclear, and whether other organs play a significant role is unknown. Furthermore, novel approaches are needed for a better understanding of the effects of Cyps on systemic inflammation.

In conclusion, the relationship between Cyps and the CD147 receptor with inflammation is reinforced in the present study. Moreover, our data suggest that, in the inflammatory process, each Cyp has a different pattern distribution in systemic inflammation in each organ. Moreover, there is a direct correlation between the degree of inflammation and the levels of specific cyclophilin in each tissue. In addition, Cyps, and specially CypA, could be considered a target in preventing inflammatory-based diseases.

Author Statement

All authors have contributed to the manuscript. Sandra Gegunde,

Manuel Cifuentes, and Rebeca Alvariño performed the research; Amparo Alfonso designed the research study and conceptualization; Sandra Gegunde and Nadia Pérez-Fuentez analysed the data; Amparo Alfonso, Manuel Cifuentes, Mercedes R Vyeites and Luis M Botana performed critical discussion. The manuscript was written through the contributions of all authors that have approved the final version of the manuscript.

Declaration of Competing Interest

The authors declare that they have no known competing financial interests or personal relationships that could have appeared to influence the work reported in this paper.

Data availability

The original contributions presented in the study are included in the article. Further inquiries can be directed to the corresponding author.

Acknowledgements

We thank Dr. Daniel Romo's group from the Baylor CPRIT Synthesis and Drug-Lead Discovery Laboratory and the Department of Chemistry and Biochemistry, Baylor University (TX, United States) for kindly supplying the GraA-derived compound.

Funding

The research leading to these results has received funding from the following FEDER cofunded-grants. From Campus Terra (USC), BreveRiesgo (2022-PU011), CLIMIGAL (2022- PU016). From Conselleria de Cultura, Educacion e Ordenación Universitaria, Xunta de Galicia, GRC (ED431C 2021/01). From Ministerio de Ciencia e Innovación ISCIII/PI19/001248, PID 2020-11262RB-C21 and Grant CPP2021-008447 funded by MCIN/AEI/10.13039/501100011033 and by The European Union NextGenerationEU/PRT. From European Union Interreg Agritox EAPA-998-2018, and H2020 778069-EMERTOX. S.G. was supported by a postdoctoral fellowship from Campus Terra co-funded by Xunta de Galicia and Universidad de Santiago de Compostela, Spain. R.A. was supported by a postdoctoral fellowship from Xunta de Galicia (ED481B-2021-038), Spain. N.P.F. was supported by a predoctoral fellowship from FIDIS, Spain.

Appendix A. Supplementary material

Supplementary data to this article can be found online at https://doi.org/10.1016/j.intimp.2023.110351.

References

[1] E. Charpentier, A. Redheuil, O. Bourron, S. Boussouar, O. Lucidarme, M. Zarai, et al., Cardiac adipose tissue volume assessed by computed tomography is a specific and independent predictor of early mortality and critical illness in COVID-19 in type 2-diabetic patients, Cardiovasc. Diabetol. 21 (1) (2022) 294.
[2] G. Cecoro, M. Annunziata, M.T. Iuorio, L. Nastri, G.L. Periodontitis, Low-grade inflammation and systemic health: a scoping review, Medicina (Kaunas) 56 (6) (2020).
[3] K. Asanuma, S. Yokota, N. Chosa, M. Kamo, M. Ibi, H. Mayama, et al., Hydrogen peroxide-induced oxidative stress promotes expression of CXCL15/Lungkine mRNA in a MEK/ERK-dependent manner in fibroblast-like synoviocytes derived from mouse temporomandibular joint, J. Oral Biosci. (2022).
[4] R.Z. Zhao, S. Jiang, L. Zhang, Z.B. Yu, Mitochondrial electron transport chain, ROS generation and uncoupling (Review), Int. J. Mol. Med. 44 (1) (2019) 3–15.
[5] M. Bukrinsky, Extracellular cyclophilins in health and disease, BBA 1850 (10) (2015) 2087–2095.
[6] G.L. Perrucci, A. Gowran, M. Zanobini, M.C. Capogrossi, G. Pompilio, P. Nigro, Peptidyl-prolyl isomerases: a full cast of critical actors in cardiovascular diseases, Cardiovasc. Res. 106 (3) (2015) 353–364.
[7] J.M. Han, H.J. Jung, Cyclophilin A/CD147 interaction: a promising target for anticancer therapy, Int. J. Mol. Sci. 23 (16) (2022).
[8] S.E. Volker, S.E. Hedrick, Y.B. Feeney, C.V. Clevenger, Cyclophilin A function in mammary epithelium impacts Jak2/Stat5 signaling, morphogenesis, differentiation, and tumorigenesis in the mammary gland, Cancer Res. 78 (14) (2018) 3877–3887.
[9] P. Stocki, D.C. Chapman, L.A. Beach, D.B. Williams, Depletion of cyclophilins B and C leads to dysregulation of endoplasmic reticulum redox homeostasis, J. Biol. Chem. 289 (33) (2014) 23086–23096.
[10] J. Friedman, I. Weissman, J. Friedman, S. Alpert, An analysis of the expression of cyclophilin C reveals tissue restriction and an intriguing pattern in the mouse kidney, Am. J. Pathol. 144 (6) (1994) 1247–1256.
[11] G. Amanakis, E. Murphy, Cyclophilin D: an integrator of mitochondrial function, Front. Physiol. 11 (2020) 595.
[12] H. Hoffmann, C. Schiene-Fischer, Functional aspects of extracellular cyclophilins, Biol. Chem. 395 (7–8) (2014) 721–735.
[13] H. Zhang, Q. Fan, H. Xie, L. Lu, R. Tao, F. Wang, et al., Elevated serum Cyclophilin B levels are associated with the prevalence and severity of metabolic syndrome, Front Endocrinol (Lausanne). 8 (2017) 360.
[14] A. Alfonso, J. Bayon, S. Gegunde, E. Alonso, R. Alvarino, M. Santas-Alvarez, et al., High Serum Cyclophilin C Levels As A Risk Factor Marker For Coronary Artery Disease, Sci. Rep. 9 (1) (2019) 10576.
[15] J. Bayon, A. Alfonso, S. Gegunde, E. Alonso, R. Alvarino, M. Santas-Alvarez, et al., Cyclophilins in ischemic heart disease: differences between acute and chronic coronary artery disease patients, Cardiol Res. 11 (5) (2020) 319–327.
[16] V. Yurchenko, S. Constant, M. Bukrinsky, Dealing with the family: CD147 interactions with cyclophilins, Immunology 117 (3) (2006) 301–309.
[17] V. Yurchenko, M. O'Connor, W.W. Dai, H. Guo, B. Toole, B. Sherry, et al., CD147 is a signaling receptor for cyclophilin B, Biochem. Biophys. Res. Commun. 288 (4) (2001) 786–788.
[18] V. Yurchenko, S. Constant, E. Eisenmesser, M. Bukrinsky, Cyclophilin-CD147 interactions: a new target for anti-inflammatory therapeutics, Clin. Exp. Immunol. 160 (3) (2010) 305–317.
[19] Y. Liao, K. Peng, X. Li, Y. Ye, P. Liu, Y. Zeng, The adhesion protein of Mycoplasma genitalium inhibits urethral epithelial cell apoptosis through CypA-CD147 activating PI3K/ Akt/NF-kappaB pathway, Appl. Microbiol. Biotechnol. 106 (19–20) (2022) 6657–6669.
[20] A.A. Hoyer, K. Klaeske, J. Garnham, P. Kiefer, A. Salameh, K. Witte, et al., Cyclosporine A-enhanced cardioplegia preserves mitochondrial basal respiration after ischemic arrest, Perfusion (2021).
[21] J. Patocka, E. Nepovimova, K. Kuca, W. Wu, Cyclosporine a: chemistry and toxicity - a review, Curr. Med. Chem. 28 (20) (2021) 3925–3934.
[22] A.H. de Wilde, U. Pham, C.C. Posthuma, E.J. Snijder, Cyclophilins and cyclophilin inhibitors in nidovirus replication, Virology 522 (2018) 46–55.
[23] S. Sivasinprasasn, N. Wikan, J. Tocharus, R. Pantan, W. Chaichompoo, A. Suksamrarn, et al., Synergistic effects of the capsaicinoid nonivamide and rosuvastatin on obesity-related endothelial dysfunction in rat fed a high-fat diet, Phytother. Res. 33 (7) (2019) 1815–1826.
[24] G. Maurizi, L. Della Guardia, A. Maurizi, A. Poloni, Adipocytes properties and crosstalk with immune system in obesity-related inflammation, J. Cell. Physiol. 233 (1) (2018) 88–97.
[25] M.E. Abbasov, R. Alvarino, C.M. Chaheine, E. Alonso, J.A. Sanchez, M.L. Conner, et al., Simplified immunosuppressive and neuroprotective agents based on gracilin A, Nat. Chem. 11 (4) (2019) 342–350.
[26] S. Gegunde, A. Alfonso, E. Alonso, R. Alvarino, L.M. Botana, Gracilin-derivatives as lead compounds for anti-inflammatory effects, Cell. Mol. Neurobiol. 40 (4) (2020) 603–615.
[27] S. Gegunde, A. Alfonso, R. Alvariño, E. Alonso, B.LM. Cyclophilins, A, B, and C role in human T lymphocytes upon inflammatory conditions, Front. Immunol. 12 (1030) (2021).
[28] C. Ortiz-Hidalgo, Abelardo Gallego (1879–1930) and his contributions to histotechnology: the Gallego stains, Acta Histochem. 113 (2) (2011) 189–193.
[29] M. Gajda, A. Jasztal, T. Banasik, E. Jasek-Gajda, S. Chlopicki, Combined orcein and martius scarlet blue (OMSB) staining for qualitative and quantitative analyses of atherosclerotic plaques in brachiocephalic arteries in apoE/LDLR(-/-) mice, Histochem. Cell Biol. 147 (6) (2017) 671–681.
[30] C.M. Lange, Systemic inflammation in hepatorenal syndrome - a target for novel treatment strategies? Liver Int. 39 (7) (2019) 1199–1201.
[31] L.M. Buja, T. Kita, J.L. Goldstein, Y. Watanabe, M.S. Brown, Cellular pathology of progressive atherosclerosis in the WHHL rabbit. An animal model of familial hypercholesterolemia, Arteriosclerosis 3 (1) (1983) 87–101.
[32] Y.X. Ru, H.C. Shang, S.X. Dong, S.X. Zhao, H.Y. Liang, C.J. Zhu, Foam cell origination from degenerated vascular smooth muscle cells in atherosclerosis: an ultrastructural study on hyperlipidemic rabbits, Ultrastruct. Pathol. 44 (1) (2020) 103–115.
[33] J.A. Sanchez, A. Alfonso, I. Rodriguez, E. Alonso, J.M. Cifuentes, R. Bermudez, et al., Spongionella secondary metabolites, promising modulators of immune response through CD147 receptor modulation, Front. Immunol. 7 (2016) 452.
[34] G.P.J. van Hout, L. Bosch, The inflammasomes in cardiovascular disease, Exp Suppl. 108 (2018) 9–40.
[35] G.H. Norris, C.M. Porter, C. Jiang, C.L. Millar, C.N. Blesso, Dietary sphingomyelin attenuates hepatic steatosis and adipose tissue inflammation in high-fat-diet-induced obese mice, J. Nutr. Biochem. 40 (2017) 36–43.
[36] Y. Wang, H. Lu, Z. Huang, H. Lin, Z. Lei, X. Chen, et al., Apolipoprotein E-knockout mice on high-fat diet show autoimmune injury on kidney and aorta, Biochem. Biophys. Res. Commun. 450 (1) (2014) 788–793.
[37] G.R. Geovanini, P. Libby, Atherosclerosis and inflammation: overview and updates, Clin. Sci. (Lond.) 132 (12) (2018) 1243–1252.

[38] V. Anandan, T. Thulaseedharan, A. Suresh Kumar, K. Chandran Latha, A. Revikumar, A. Mullasari, et al., Cyclophilin a impairs efferocytosis and accelerates atherosclerosis by overexpressing CD 47 and down-regulating calreticulin, Cells. 10 (12) (2021).
[39] M. Terajima, Y. Taga, W.A. Cabral, M. Nagasawa, N. Sumida, S. Hattori, et al., Cyclophilin B deficiency causes abnormal dentin collagen matrix, J. Proteome Res. 16 (8) (2017) 2914–2923.
[40] R. Alvarino, A. Alfonso, N. Perez-Fuentes, J.M. Gonzalez-Jartin, S. Gegunde, M. R. Vieytes, et al., Extracellular cyclophilins A and C induce dysfunction of pancreatic microendothelial cells, Front. Physiol. 13 (2022), 980232.
[41] L. Zhang, Z. Li, B. Zhang, H. He, Y. Bai, PPIA is a novel adipogenic factor implicated in obesity, Obesity (Silver Spring) 23 (10) (2015) 2093–2100.
[42] X. Li, M. Yang, H. Sun, M.R.U. Ferdous, L. Gao, J. Zhao, et al., Liver cyclophilin D deficiency inhibits the progression of early NASH by ameliorating steatosis and inflammation, Biochem. Biophys. Res. Commun. 594 (2022) 168–176.
[43] X. Su, D. Lin, D. Luo, M. Sun, X. Wang, J. Ye, et al., Cyclophilin D participates in the inhibitory effect of high-fat diet on the expression of steroidogenic acute regulatory protein, J. Cell Mol. Med. 23 (10) (2019) 6859–6871.
[44] C. Lebeaupin, D. Vallee, Y. Hazari, C. Hetz, E. Chevet, B. Bailly-Maitre, Endoplasmic reticulum stress signalling and the pathogenesis of non-alcoholic fatty liver disease, J. Hepatol. 69 (4) (2018) 927–947.
[45] K. Zuzda, W. Grycuk, J. Malyszko, J. Malyszko, Kidney and lipids: novel potential therapeutic targets for dyslipidemia in kidney disease? Exp. Opin. Ther. Targets 1–15 (2022).
[46] K.G. Leong, E. Ozols, J. Kanellis, D.J. Nikolic-Paterson, F.Y. Ma, Cyclophilin A promotes inflammation in acute kidney injury but not in renal fibrosis, Int. J. Mol. Sci. 21 (10) (2020).
[47] M. Nakai, A. Shimokado, T. Kubo, Y. Katayama, T. Nishiguchi, M. Kashiwagi, et al., Expression of Cyclophilin a in coronary artery plaque with intraplaque hemorrhage is more frequent in deceased patients who had impaired kidney function, Int. Heart J. 61 (6) (2020) 1129–1134.
[48] R. Cabello, M. Fontecha-Barriuso, D. Martin-Sanchez, A.M. Lopez-Diaz, S. Carrasco, I. Mahillo, et al., Urinary cyclophilin a as marker of tubular cell death and kidney injury, Biomedicines. 9 (2) (2021).
[49] M.J. Bergeron, M. Burzle, G. Kovacs, A. Simonin, M.A. Hediger, Synthesis, maturation, and trafficking of human Na+-dicarboxylate cotransporter NaDC1 requires the chaperone activity of cyclophilin B, J. Biol. Chem. 286 (13) (2011) 11242–11253.
[50] B. Wang, L. Lin, H. Wang, H. Guo, Y. Gu, W. Ding, Overexpressed cyclophilin B suppresses aldosterone-induced proximal tubular cell injury both in vitro and in vivo, Oncotarget 7 (43) (2016) 69309–69320.
[51] S. Gegunde, A. Alfonso, R. Alvarino, E. Alonso, C. Gonzalez-Juanatey, L.M. Botana, Crosstalk between cyclophilins and T lymphocytes in coronary artery disease, Exp. Cell Res. 400 (2) (2021), 112514.
[52] J. Geng, L. Chen, Y. Yuan, K. Wang, Y. Wang, C. Qin, et al., CD147 antibody specifically and effectively inhibits infection and cytokine storm of SARS-CoV-2 and its variants delta, alpha, beta, and gamma, Signal Transduct. Target. Ther. 6 (1) (2021) 347.
[53] S. Ramachandran, A. Vinitha, C.C. Kartha, Cyclophilin A enhances macrophage differentiation and lipid uptake in high glucose conditions: a cellular mechanism for accelerated macro vascular disease in diabetes mellitus, Cardiovasc. Diabetol. 15 (1) (2016) 152.
[54] J. Lou, C. Li, Z.S. Li, T. Zhang, Z.N. Chen, H. Bian, Hepatic CD147 knockout modulates liver steatosis and up-regulates autophagy in high-fat-diet-induced NAFLD mice, Biochem. Biophys. Res. Commun. 524 (4) (2020) 1010–1017.
[55] T. Kosugi, K. Maeda, W. Sato, S. Maruyama, K. Kadomatsu, CD147 (EMMPRIN/Basigin) in kidney diseases: from an inflammation and immune system viewpoint, Nephrol. Dial. Transplant. 30 (7) (2015) 1097–1103.
[56] F. Lamoureux, L.N. Gastinel, E. Mestre, P. Marquet, M. Essig, Mapping cyclosporine-induced changes in protein secretion by renal cells using stable isotope labeling with amino acids in cell culture (SILAC), J. Proteom. 75 (12) (2012) 3674–3687.
[57] J. Kuo, S.S. Serrano, A. Gronberg, R. Massoumi, M.J. Hansson, P. Gallay, Cyclophilin inhibitor NV556 reduces fibrosis and hepatocellular carcinoma development in mice with non-alcoholic steatohepatitis, Front. Pharmacol. 10 (2019) 1129.
[58] S.A. Harrison, P.R. Mayo, T.M. Hobbs, C. Canizares, E.P. Foster, C. Zhao, et al., Rencofilstat, a cyclophilin inhibitor: a phase 2a, multicenter, single-blind, placebo-controlled study in F2/F3 NASH, Hepatol Commun. 6 (12) (2022) 3379–3392.
[59] J. Colgan, M. Asmal, B. Yu, J. Luban, Cyclophilin A-deficient mice are resistant to immunosuppression by cyclosporine, J. Immunol. 174 (10) (2005) 6030–6038.
[60] O. Cho, Y. Matsumoto, T. Yamada, T. Sugita, Establishment of a gene recombination method for a major human skin commensal fungus, Malassezia restricta, using Agrobacterium tumefaciens-mediated gene transfer system, Med. Mycol. 60 (11) (2022).